Topological MRI Prostate Segmentation Method

Done Stojanov
Faculty of Computer Science,
University Goce Delcev-Stip
ul. Krste Misirkov 10/A, 2000 Stip, Macedonia
Email: done.stojanov@ugd.edu.mk

Saso Koceski
Faculty of Computer Science,
University Goce Delcev-Stip
ul. Krste Misirkov 10/A, 2000 Stip, Macedonia
Email: saso.koceski@ugd.edu.mk

Abstract—**The main aim of this paper is to advance the state of the art in automated prostate segmentation using T2 weighted MR images, by introducing a hybrid topological MRI prostate segmentation method which is based on a set of pre-labeled MR atlas images. The proposed method has been experimentally tested on a set of 30 MRI T2 weighted images. For evaluation the automated segmentations of the proposed scheme have been compared with the manual segmentations, using an average Dice Similarity Coefficient (DSC). Obtained quantitative results have shown a good approximation of the segmented prostate.**

Keywords: Prostate segmentation, MRI T2, hybrid topological method

I. Introduction

PROSTATE cancer is one of the major healthcare problems affecting men's population and is the second most common cancer in men worldwide. An estimated 1.1 million men worldwide were diagnosed with prostate cancer in 2012, accounting for 15% of the cancers diagnosed in men. Considering this worrying data, it is predicted that the number of cases will almost double by 2030 [1]. Consequently, there is an increased demand and interest in advancements and enhancements of current methodologies for prostate cancer diagnosis and treatment planning.

Determination of proper information about the prostate location, its volume and shape of prostate gland are basic task and play essential role in numerous clinical applications. This information is crucial for cancer detection, localization and staging, guided biopsy, radiation treatment planning, but also for surgical planning and image-guided robotic-aided laparoscopic prostatectomy (RALP) with augmented reality (AR). In order to provide accurate information various imaging techniques are used in the clinical practice. Nowadays, trans rectal ultrasound (TRUS) is probably the most common and widespread medical imaging technique employed for cancer detection [2], [3], [4] as well as for guided needle biopsy [5]. This is mainly due to its low cost, portability and real-time acquisition. However, this technique has its own drawbacks. Namely, due to the low sensitivity prostate cancer visualization is poor, its false negative rate is high [6] and often resulting in high rates of rebiopsies.

Therefore, the Computer Tomography (CT) has been proposed as an alternative, and it is mainly used in prostate brachytherapy to determine the placement of the radioactive seeds and also to confirm the seed location post-procedure [7]. On the other hand, CT requires ionising radiation and nephrotoxic contrast media and could not provide differentiation between external and internal prostate anatomy because of the poor soft-tissue resolution.

Therefore, in the last decade high-resolution MRI have been promoted as a valuable alternative to before mentioned imaging techniques, which offers physicians better evaluation of the prostate diseases. In the clinical practice nowadays three different modalities of MR images are normally produced: T2-weighted, diffusion-weighted and dynamic contrast enhanced images. Recently, many scientific works have proved that MRI has very high accuracy in the detection of prostate diseases [8], [9] significantly improving the diagnostic rates. It enables easier image segmentation and determination of prostate shape and boundaries which is the basic step in clinical applications.

Usual MRI prostate examination results with a series of multiple images which are presenting plenty of anatomical and functional data regarding the prostate tissues. Analysis and segmentation of these images in major percentage of the cases in the clinical practice, currently is performed by experienced radiologists who based on their knowledge of the anatomy.

However, manual segmentation of prostate boundaries on multiple images in the MRI series could be extremely difficult and time consuming task, especially for series containing large number of images. Manual segmentation is subjective and could be performed differently by different experts and thus could produce different outcomes.

Because of this, currently there is a huge demand for fast and accurate automatic or semi-automatic segmentation methods for clinical applications.

Development of automatic segmentation algorithms and methodologies faces huge challenges, mainly owing to variability of prostate size and shape from patient to patient,

variable intensity ranges inside the prostate region and tissues of surrounding organs, as well as the absence of clear prostate boundaries.

The main aim of this paper is to advance the state of the art in automated prostate segmentation using T2 weighted MR images, by introducing a topological MRI prostate segmentation method using a set of pre-labeled MR atlas images.

The rest of the paper is organized as follows: in part II we present the current state of the art in automatic medical image segmentation methods, in part III we present the proposed topological method for MR image segmentation, in part IV the evaluation of the proposed method its results and findings about its efficiency are presented. Part V presents the work conclusions and the references are in part VI.

II. Related Work

Prostate segmentation methods based on images acquired using ultrasound, magnetic resonance and computed tomography could be generally divided into four major categories: contour and shape based methods, region based methods, supervised and un-supervised classification methods, hybrid methods [2].

Contour and shape based methods are using the boundary features to segment the prostate. This is very difficult problem since MRI exhibits high soft tissue contrast. To cope with this Zwiggelaar et al. [10] used first and second order Lindeberg directional derivatives, in a polar coordinate system to identify the edges. On the other hand, Samiee et al. [11] used prior information of the prostate shape to refine the prostate boundary. Without prior shape information segmentation was error prone and often significantly different from the anatomical structure. Therefore, Cootes et al. [12] proposed to segment prostate in MR slices using the active shape model (ASM). Slightly different approach which combines two and three dimensional ASMs to segment the prostate using MR images was proposed by Zhu et al. [13]. A three dimensional ASM was built that represented the shape variance of the prostate.

One of the commonly used methods for region based segmentation is the one which lies upon the set of manual segmentations of anatomical structures registered to a common coordinate frame called atlas, which is afterwards used as a reference. These methods are trying to map the pre-segmented images to the querying image by finding a one to one transformation. However, due to variations in image intensities and differences in shapes this matching remains to be a challenging research topic.

For this purposes, various multi-atlas segmentation methods have been analyzed in order to improve the selection of the atlas images which are most similar to the querying one [14]. It should be stressed that the weighting coefficients should favor the atlas images which are most similar to the querying one and thus should contribute more in the segmentation.

Having in mind this, Klein et al. [15] has proposed a multi-atlas approach to segment the prostate using localized mutual information. The registration of the training volumes to the querying one was performed using affine and non-rigid registration.

Álvarez et al. [16] improved this method by taking the advantage of both the inter-individual shape variation and intra-individual salient point representation.

Langerak et al. [17] focused their work pre-selection of atlases before registration by assigning them to clusters and registering only some of these clusters. They are analyzing and registering instances from each cluster and then combining them to an estimate of the target segmentation. By doing so, they claim to achieve the same accuracy with atlas reduction of even 60%.

Sjöberg and Ahnesjö [18] proposed a new multi-atlas based segmentation using probabilistic label fusion with adaptive weighting of image similarity measures. Namely, their method is based on probabilistic weighting of distance maps. Relationships between image similarities and segmentation similarities are estimated in a learning phase and used to derive fusion weights that are proportional to the probability for each atlas to improve the segmentation result.

Xie and Ruan [19] recently proposed a method where they first perform an affine registration to minimize the global mean squared error to coarsely align each atlas image to the target. Afterwards, they use a target-specific regional mean squared error, in order to select a relevant subset from the training atlas. Then non-rigid registration between the training images and the querying one are performed inside previously identified subset only. At the end, using the estimated deformation fields, structure labels are transferred from training to querying images and they are fused based on a weighted combination of regional and local mean squared error, with proper total-variation-based spatial regularization.

Makni et al. [20] proposed a modified alternative of the evidential C-means algorithm to cluster voxels in multispectral MRI, including T2 weighted, diffusion weighted and contrast enhanced images.

In contract to the previously mentioned methods, hybrid ones are combining a priory boundary and feature information. These methods are proven to give superior results in contrast to others in presence of shape and texture variations.

Vikal et al. [21] proposed a method for building an average shape model using the prior shape and size information from manually marked contours. In order to reduce the noise and enhance the contrast they used a stick filter. On the enhanced images they detected the edges by applying the Canny filter. The constructed average shape model was used to discriminate pixels which are out of the model orientation. By applying polynomial interpolation the contour was further refined. The segmented contours obtained in the middle slices were used to initialize other slices towards the peripheral zones in both directions.

III. METHODOLOGY

In order to enable accurate multi-atlas based prostate segmentation, the proposed methodology relies on most similar atlases which can provide robust and precise transformation to the target image. The proposed methodology consists of several steps as presented on the diagram in Fig. 1.
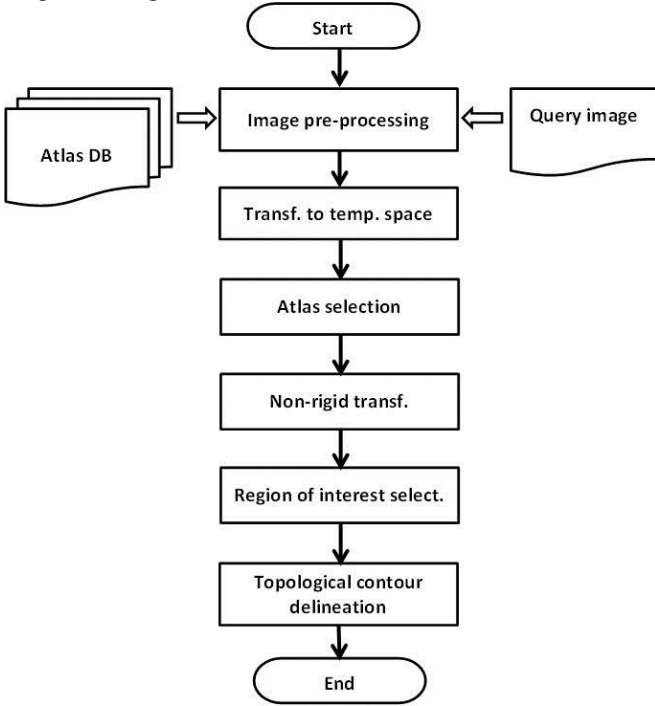

Fig. 1 Activity diagram which describes the whole methodology

Initial step of the proposed method are similar to those proposed in [15], namely appearance-specific atlas selections and a patch-based local weighting strategy for atlas fusion. After some image preprocessing which aims at inhomogeneity correction the top 5 similar atlases are selected for atlas registration based on the intensity differences in the surrounding region of the prostate. Once selected, the similar atlases are non-rigidly registered to a target image. Using the calculated transformation anatomical structure labels of the atlas are propagated to the space of the querying image. The aim of this step in our methodology is to order to derive a region of interest formed by the interception and union of the a priori shapes in the selected atlases, where the prostate contour of a non-segmented sample is supposed to be positioned. The final step is to delineate the prostate contour in the determined region by pixel classification. Namely, pixels within the region of interest are classified as prostate-likely-belonging pixels or prostate-unlikely-belonging pixels, taking into consideration the number of same-position pixels, being part of segmented samples and the intensity difference between a pixel of a non-segmented sample and the same-position pixels of segmented samples. The prostate contour is found as a set of pixels, separating column pixels (row pixels) within the

region of interest in two disjunctive sets, having maximized the number of prostate-unlike-belonging pixels in the first set and the number of prostate-likely-belonging pixels in the other set exclusively. Prostate contour of a non-segmented sample is determined in three steps, described as follows:

Step 1: Determine prostate interception and union shape model, according to Definition 1 and Definition 2, over a set of segmented samples, acquiring prostate shapes' knowledge of n segmented same size and type prostate MR images.

Definition 1: A pixel $p[i, j]$ is an interception model pixel if:

$ss_1[i, j] \in$ prostate segment ss_1,

$ss_2[i, j] \in$ prostate segment ss_2,

…

$ss_{n-1}[i, j] \in$ prostate segment ss_{n-1},

$ss_n[i, j] \in$ prostate segment ss_n,

where $ss_i, 1 \leq i \leq n$ is a segmented sample.

Definition 2: A pixel $p[i, j]$ is a union model pixel if:

$ss_1[i, j] \in$ prostate segment ss_1 or

$ss_2[i, j] \in$ prostate segment ss_2 or

…

$ss_{n-1}[i, j] \in$ prostate segment ss_{n-1} or

$ss_n[i, j] \in$ prostate segment ss_n,

where $ss_i, 1 \leq i \leq n$ is a segmented sample.

According to previous definitions, if a pixel at position i,j is found as a prostate pixel in all segmented samples, then the pixels is considered as a part of the interception model. If at least one pixel at position i,j is found as a prostate pixel, then the pixel is a union model pixel. Interception pixels are considered as a part of the prostate of a non-segmented MR image.

Step 2: Classify each pixel within the union, but out of the interception as a prostate-likely-belonging pixel or prostate-unlikely-belonging pixel, exclusively according Eq. 1 and Eq.2.

If Eq.1 is satisfied,

$$(n - n_{plb})\text{diff}_{plb} \leq (n - n_{pulb})\text{diff}_{pulb} \qquad (1)$$

classify the pixel $p[i, j]$ as a prostate-likely-belonging pixel.

If Eq.2 is satisfied,

$$(n - n_{plb})\text{diff}_{plb} > (n - n_{pulb})\text{diff}_{pulb} \qquad (2)$$

classify the pixel $p[i, j]$ as a prostate-unlikely-belonging pixel.

Equation 1, 2 parameters are the following ones:

n : Number of segmented samples.

n_{plb}: Number of segmented samples, where pixel at position i,j is part of the prostate segmented region.

n_{pulb}: Number of segmented samples, where pixel at position i,j is not a prostate pixel.

The intensity difference between a pixel $p[i, j]$ of a non-segmented sample and the mean intensity of pixels at position i,j, part of a prostate in segmented samples, is calculated according Eq. 3.

$$\text{diff}_{plb} = p[i, j] - (\sum_{k=1}^{n} ss_k[i, j]) / n_{plb} \qquad (3)$$

where $ss_k[i, j] \in$ prostate segment of ss_k

The intensity difference between a pixel $p[i, j]$ of a non-segmented sample and the mean intensity of pixels at position i,j, out of the prostate in segmented samples, is calculated according Eq. 4.

$$\text{diff}_{pulb} = p[i, j] - (\sum_{k=1}^{n} ss_k[i, j]) / n_{pulb} \qquad (4)$$

where $ss_k[i, j] \notin$ prostate segment of ss_k

Value-opposite differences: $(n - n_{plb})$ and $(n - n_{pulb})$ serve as a weight factor for pixel intensity differences: diff_{plb} and diff_{pulb}. The smaller $(n - n_{plb})$ is, greater difference $(n - n_{pulb})$ is obtained. Relatively small pixel intensity difference diff_{plb} increases pixel prostate belonging expectation. On the contrary, small pixel intensity difference diff_{pulb} decreases pixel prostate belonging expectation. Combining previous parameters in a single equation (Equations 1, 2), a prostate pixel classifier is derived.

Step 3: Determine prostate contour shape as a set of pixel, separating the union, out of the interception in two disjunctive sets, such as the number of prostate-unlike-belonging pixels in the first set and the number of prostate-likely-belonging pixels in the other set is exclusively maximized.

Applying Equations 1, 2 for pixels of a non-segmented sample, out of the interception, but within the union, each pixel in the region is classified as a prostate-likely-belonging or prostate-unlikely-belonging pixel, exclusively.

Representing with 1 prostate-likely-belonging classified pixels, while with 0 prostate-unlikely-belonging classified pixels, the problem of identification of a prostate contour pixel is simplified to identification of prostate contour pixels, separating same row pixels (same column pixels), out of the interception, but within the union, in two disjunctive sets, such as the number of prostate-unlikely-belonging pixels and prostate-likely-belonging pixels in the sets is exclusively maximized.

For example, if $CP = \begin{bmatrix} p[i, j] \\ p[i+1, j] \\ p[i+2, j] \\ p[i+3, j] \\ p[i+4, j] \\ p[i+5, j] \end{bmatrix}$ is a six pixel same column set, out of the interception, but within the union, being accordingly classified as: $CCP = \{0,1,0,0,1,1\}$, there are 4 prostate contour candidate pixels, without taking into consideration the first and the last pixel. Pixel $p[i+1, j]$ separates classified set CPP in two disjunctive sets: $CPP_1 = \{0,1\}$, $CPP_2 = \{0,0,1,1\}$. The number of prostate-unlikely-belonging pixels in the first set is 1, while the number of prostate-likely-belonging pixels in the second set is 2. The sum equals 3. Similarly, pixel $p[i+2, j]$ separates set CPP in two disjunctive sets: $CPP_1 = \{0,1,0\}$, $CPP_2 = \{0,1,1\}$. Now the number of prostate-unlikely-belonging pixels in the first set is 2, while the number of prostate-likely-belonging pixels in the second set is 2. The sum equals 4. Choosing pixel $p[i+3, j]$ as a prostate contour pixel, the following disjunctive sets are obtained: $CPP_1 = \{0,1,0,0\}$, $CPP_2 = \{1,1\}$. The number of prostate-unlikely-belonging pixels in the first set is 3, while the number of prostate-likely-belonging pixels in the second set is 2. Their sum equals 5. Pixel $p[i+4, j]$ assumed as a prostate contour pixel, decreases the number of prostate-likely-belonging pixels in CPP_2 , while the number of prostate-unlikely belonging pixels in CPP_1 remains unchanged.

Therefore, pixel $p[i+3, j]$ is chosen as a prostate contour pixel, since the sum of prostate-unlikely-belonging pixel and prostate-likely-belonging pixels in the disjunctive sets is maximized in that case (Fig.2).

-1	-1	-1
-1	8	-1
-1	-1	-1

Fig. 2 Point detection mask

If the condition given by Eq.5 is satisfied

$$R = \frac{1}{8}(8\,p[i, j] - p[i-1, j-1] - p[i-1, j] -$$
$$p[i-1, j+1] - p[i, j-1] - p[i, j+1] - \qquad (5)$$
$$p[i+1, j-1] - p[i+1, j] - p[i+1, j+1]) > T$$

then the pixel p[i, j] is a prostate contour outlying pixel.

Discontinuous prostate contour curves are linked together applying standard image morphological operations, such as multiple Dilatation at first, then Erosion, in order to derive one pixel-thin prostate contour. Figure 3 represents the structuring element used in the morphological operations.
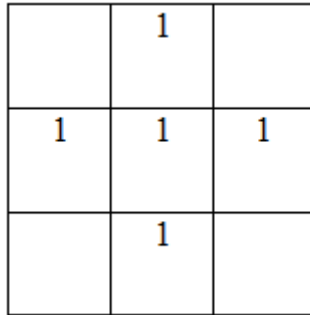

Fig. 3 Morphological operations' structuring element

IV. EXPERIMENTAL EVALUATION AND RESULTS

For evaluation purposes all the steps described of the proposed methodology and presented in Fig. 1 are implemented in C# programming language. The program was executed on laptop with 4GB RAM memory and equipped with Intel Core i3 CPU with 2.4GHz and 64 bit Windows 7 OS. It has also ATI Mobility Radeon HD 4650 with 1GB dedicated memory. The proposed method was evaluated on 30 training MRI prostate images. The image series used for this evaluation were T2 FSE AXIALS 256x256 pixel. They were obtained from the online Prostate MR Image Database [22]. For each training image, manual segmentation is provided.

A leave-one-out study has been implemented based on each of the training scans using the remaining 29 images as the atlas database. In the sub-database, the top 5 most similar atlases are chosen. Based on these atlases the union and the interception shape model are constructed.

For better visual representation of the obtained results the following coloring convention was used: the red colored region represents the interception model, while the white colored region represents the union, out of the interception, Figure 4.

Pixels within the interception are considered as a part of the prostate. Each pixel within the white colored region is exclusively classified as a prostate-likely-belonging pixel or prostate-unlikely-belonging pixel.

Taking image 000046.00001.001.0013 from the Prostate MR Image Database (http://prostatemrimagedatabase.com/Database/000046/00001/001/0013.html) as a querying image, the result of the classification is shown on Figure 5. Red pixels, out of the interception, but within the union are classified as prostate-likely-belonging pixels, satisfying Equation 1, while the white pixels in the same region are classified as prostate-unlikely-belonging pixels, satisfying Equation 2.
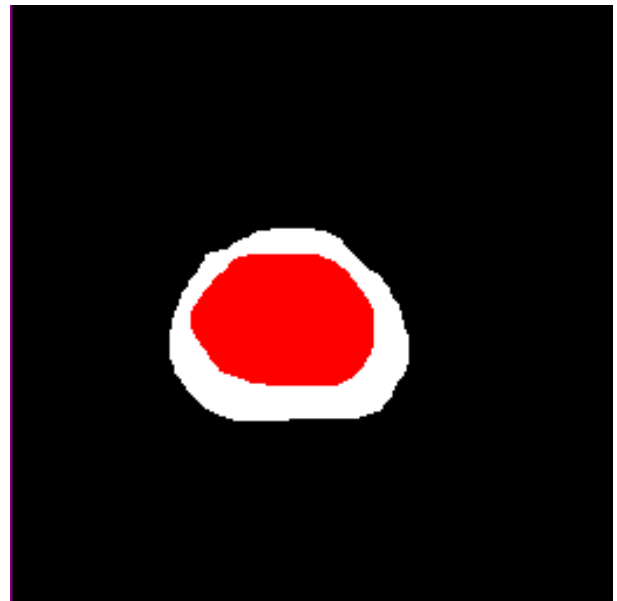

Fig. 4 Interception and union derived model

In Figure 5 blue colored pixels are the prostate contour pixels, determined in the third processing step of the proposed method.

Filtering prostate contour outlying pixels and applying standard region closing morphological operation, using Figure 3 structuring element, the prostate contour of a non-segmented T2 FSE AXIALS database image 000046.00001.001.0013 is obtained, Figure 6.
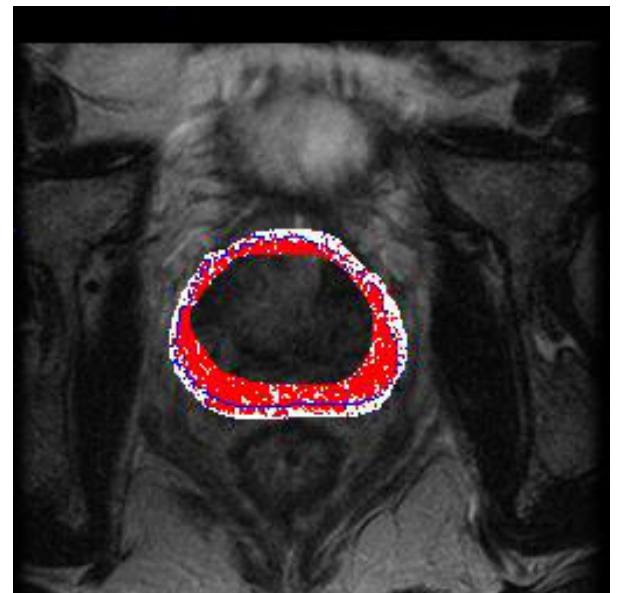
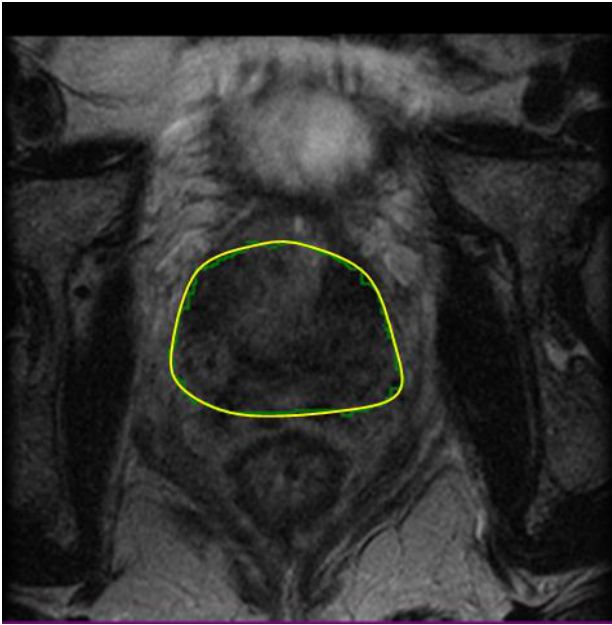

Fig. 5 Method application results

Fig. 6 Identified prostate contour (green), gold standard contour delineated manually by the expert (yellow).

For evaluation of the proposed method, we have used Dice similarity coefficient (DSC) defined as in Eq. 6 compared with the manual expert segmentation.

$$DSC = 2 \cdot \frac{A \cap B}{A + B} \qquad (6)$$

It has been applied on the apex, central and the base region of the prostate. The average of this metric with its standard deviations calculated from the selected image series compared with the corresponding manual segmentation is given in Table1.

TABLE I.
PROSTATE SEGMENTATION QUANTITATIVE RESULTS FOR TRAINING DATASETS

Region	DSC
Apex	0.81±0.13
Central	0.82±0.10
Base	0.79±0.17

V. CONCLUSION

Comparing the obtained results a conclusion for prostate shape accordance can be derived, based on the prostate edges' direction compatibility, prostate contour position and prostate surface.

In general, prostate segmentation result in this case depends of two factors. The number of segmented samples used and segmented samples' prostate shape variability, based on what the interception and the union shapes are determined. More segmented samples are considered, with wider prostate shape variability, more accurate prostate contour is obtained. A drawback of the proposed method is the incapacity of detecting prostate segments, out of the derived union region, being part of prostate of a non-segmented sample. On the opposite, prostate segmentation running time is significantly improved, since relatively small segment of a non-segmented prostate MR image is processed.

REFERENCES

[1] GLOBOCAN 2012 (online at http://globocan.iarc.fr, last visited 19.04.2014).
[2] Ghose, S., Oliver, A., Martí, R., Lladó, X., Vilanova, J. C., Freixenet, J., Mitra, J., Sidibé, D., Meriaudeau, F. A survey of prostate segmentation methodologies in ultrasound, magnetic resonance and computed tomography images. Computer methods and programs in biomedicine, 108(1), 262-287, 2012, http://dx.doi.org/10.1016/j.cmpb.2012.04.006
[3] Kim, S. G., Seo, Y. G., A TRUS Prostate Segmentation using Gabor Texture Features and Snake-like Contour. Journal of Information Processing Systems, 9(1), 2013, http://dx.doi.org/10.3745/JIPS.2013.9.1.103
[4] Natarajan, S., Marks, L. S., Margolis, D. J., Huang, J., Macairan, M. L., Lieu, P., & Fenster, A. Clinical application of a 3D ultrasound-guided prostate biopsy system. In Urologic Oncology: Seminars and Original Investigations, Vol. 29, No. 3, pp. 334-342, June 2011, Elsevier, http://dx.doi.org/10.1016/j.urolonc.2011.02.014
[5] Woodruff, A.J., Morgan, T.M., Wright, J.L., Porter, C.R.., Prostate volume as an independent predictor of prostate cancer and high-grade disease on prostate needle biopsy. J Clin Oncol 26: 5165, 2008
[6] Catalona, W. J., Smith, D. S., Ratliff T. L., Dodds, K. M., Coplen, D. E., Yuan, J. J., Petros, J.A., Andriole, G. L., "Measurement of prostate-specific antigen in serum as a screening test for prostate cancer", New England Journal of Medicine, vol. 324, no. 17, pp. 1156–1161, 1991, http://dx.doi.org/10.1056/NEJM199104253241702
[7] Halpern, E. J., Cochlin, D. L., Goldberg, B. B., Imaging of the prostate, Informa Healthcare, United Kingdom, first edition, 2002
[8] Ozer, S., Langer, D. L., Liu, X., Haider, M. A., Van der Kwast, T. H., Evans, A. J., Yang, Y., Wernick, M. N., Yetik,I. S., Supervised and Unsupervised Methods for Prostate Cancer Segmentation with Multispectral MRI, Medical Physics 37 (2010) 1873–83, http://dx.doi.org/10.1118/1.3359459
[9] Puech, P., Betrouni, N., Makni, N., Dewalle, A.S., Villers, A., Lemaitre, L., Computer-Assisted Diagnosis of Prostate Cancer Using DCE-MRI Data: Design, Implementation and Preliminary Results, International Journal of Computer Assisted Radiology and Surgery 4 (2009) 1–10, http://dx.doi.org/10.1007/s11548-008-0261-2
[10] Zwiggelaar, R., Zhu, Y., Williams, S., Semi-Automatic Segmentation of the Prostate, in: F. J. Perales, A. J. Campilho, N. P. de la Blanca, A. Sanfeliu (Eds.), Pattern Recognition and Image Analysis, Proceedings of First Iberian Conference, IbPRIA, Springer, Berlin and Heidelberg and New York and Hong Kong and London and Milan and Paris and Tokyo, 2003, pp. 1108–16, http://dx.doi.org/10.1007/978-3-540-44871-6_128
[11] Samiee, M., Thomas, G., Fazel-Rezai, R., Semi-Automatic Prostate Segmentation of MR Images Based on Flow Orientation, in: IEEE International Symposium on Signal Processing and Information Technology, IEEE Computer Society Press, USA, 2006, pp. 203–7, http://dx.doi.org/10.1109/ISSPIT.2006.270797
[12] Cootes, T. F., Hill, A., Taylor, C. J., Haslam, J., The Use of Active Shape Model for Locating Structures in Medical Images, Image and

Vision Computing 12 (1994)355–66,
http://dx.doi.org/10.1007/BFb0013779

[13] Zhu, Y., Williams, S., Zwiggelaar, R., A Hybrid ASM Approach for Sparse Volumetric Data Segmentation, Pattern Recognition and Image Analysis 17 (2007) 252–8, http://dx.doi.org/10.1134/S1054661807020125

[14] Ghose, S., Oliver, A., Marti, R., Llado, X., Freixenet, J., Vilanova, J. C., Meriaudeau, F. A probabilistic framework for automatic prostate segmentation with a statistical model of shape and appearance. In Image Processing (ICIP), 2011 18th IEEE International Conference on (pp. 713-716). 2011, September IEEE, http://dx.doi.org/10.1109/ICIP.2011.6116653

[15] Klein, S., Van der Heide, U. A., Lipps, I. M., Vulpen, M. V., Staring, M., Pluim, J. P. W.,"Automatic Segmentation of the Prostate in 3D MR Images by Atlas Matching Using Localized Mutual Information", Medical Physics 35 (2008) 1407–17, http://dx.doi.org/10.1118/1.2842076

[16] Álvarez, C., Martínez, F., Romero, E., "A novel atlas-based approach for MRI prostate segmentation using multiscale points of interest ", Proc. SPIE 8922, IX International Seminar on Medical Information Processing and Analysis, 89220O (November 19, 2013), http://dx.doi.org/10.1117/12.2035462

[17] Langerak, T. R., Berendsen, F. F., Van der Heide, U. A., Kotte, A. N., Pluim, J. P. Multiatlas-based segmentation with preregistration atlas selection. Medical physics, 40(9), 2013, 091701, http://dx.doi.org/10.1118/1.4816654

[18] Sjöberg, C., & Ahnesjö, A. Multi-atlas based segmentation using probabilistic label fusion with adaptive weighting of image similarity measures. Computer methods and programs in biomedicine, 110(3), 2013, pp.308-319, http://dx.doi.org/10.1016/j.cmpb.2012.12.006

[19] Xie, Q., Ruan, D. Low-complexity atlas-based prostate segmentation by combining global, regional, and local metrics. Medical physics, 41(4), 2014, 041909, http://dx.doi.org/10.1118/1.4867855

[20] Makni, N., Iancu, A., Colot, O., Puech, P., Mordon, S., Betrouni, N., et al.: Zonal segmentation of prostate using multispectral magnetic resonance images. Medical Physics 38(11), 6093 (2011), http://dx.doi.org/10.1118/1.3651610

[21] Vikal, S., Haker, S., Tempany, C., Fichtinger, G., Prostate Contouring in MRI Guided Biopsy, in: J. P. W. Pluim, B. M. Dawant (Eds.), Proceedings of SPIE Medical Imaging: Image Processing, SPIE, USA, 2009, pp. 7259–72594A, http://dx.doi.org/ 10.1117/12.812433.

[22] Prostate MR Image Database, The Brigham and Women's Hospital, 2008 (Online at: http://prostatemrimagedatabase.com; last accessed 19.04.2014).